

Quantifying the Morphology of Calcareous Sands by Dynamic Image Analysis

Houzhen Wei¹, Tao Zhao², Qingshan Meng³, Xinzhi Wang⁴, and Bin Zhang⁵

¹Associate Professor, State Key Laboratory Geomechanics and Geotechnical Engineering, Institute of Rock and Soil Mechanics, Chinese Academy of Sciences, Wuhan, 430071, China. E-mail: hzwei@whrsm.ac.cn

²Lecturer, Department of Civil and Environmental Engineering, Brunel University London, London, UB8 3PH, United Kingdom (corresponding author). E-mail: tao.zhao@brunel.ac.uk

³Professor, State Key Laboratory Geomechanics and Geotechnical Engineering, Institute of Rock and Soil Mechanics, Chinese Academy of Sciences, Wuhan, 430071, China. E-mail: qsmeng@whrsm.ac.cn

⁴Associate Professor, State Key Laboratory Geomechanics and Geotechnical Engineering, Institute of Rock and Soil Mechanics, Chinese Academy of Sciences, Wuhan, 430071, China. E-mail: xzawang@whrsm.ac.cn

⁵Engineer, China Petroleum Pipeline International, North Yinhe Road, Langfang, 065000, China. E-mail: 747025917@qq.com

Abstract: It is commonly accepted that the macro-response of soil depends significantly on the microscopic particle characteristic features, such as size, shape and roughness. These parameters can be readily obtained by dynamic image analysis on each individual particle, enabling the quantification of particle morphologies. This study investigates the variation of calcareous sand morphology before and after the one-dimensional normal compression. The tests employ a large oedometer cell (of 231.6 mm inner diameter and 155 mm in height) and coarse calcareous particles (sizes of 10 – 20 mm). It was found that samples of different particle shape mixtures have almost the same compressibility due to continuous breakage and gradual fining of coarse sand particles. The particle breakage can be effectively quantified by the change of total particle perimeters in the dynamic image analysis. The mixture of branched particles in blocky sands can effectively increase the particle breakage factor because the branched structure can be easily crushed due to localized stresses during the compression. The breakage of coarse particles can produce a large number of fine particles with an exponential frequency distribution (by number). These fine particles are generally more elongated and flatter than the coarser ones. After the compression tests, all particles tend to be slightly smoother and more spherical, due mainly to the particle asperity damage. In particular, the rounded (spherical) particles are much smoother than the angular ones. The relevance of particle morphology change to geotechnical engineering practice is also established.

Keywords: Particle morphology; calcareous sand; normal compression; particle breakage

Introduction

The breakage of sand particles has been widely observed in many geotechnical engineering practices such as dynamic compaction, pile driving and overloading. Among others, changes

of grading, shape and surface roughness are the most notable characteristics of particle breakage (Cavarretta et al., 2017, Lade et al., 1996, Wei et al., 2018, Xiao et al., 2018). It often has a significant influence on the parameters of final product performance such as bulk packing density, flowability, internal friction angle and compressibility (Xiao et al., 2019). In particular, particle breakage has been identified to have a fundamental influence on the yielding, plastic deformation and critical state behaviour of soil (Cheng et al., 2004, Wood and Maeda, 2007, Xiao et al., 2016, Xiao et al., 2019). Therefore, quantifying particle breakage and morphology are required for comprehensive analyses of the macroscopic soil behaviour and reliable constitutive models (Chen et al., 2015, Cil and Alshibli, 2014, Ghafghazi et al., 2014, Hyodo et al., 2002, Kikumoto et al., 2010, McDowell and Bolton, 1998, Xiao and Liu, 2017).

Coop and Lee (1993) has identified a unique linear relationship between the relative particle breakage factor, B_r (see the definition in Hardin (1985)), and the logarithm of mean normal effective stress. This relationship is independent of the initial packing density and the loading stress path. However, the particle grading can change significantly as many fine particles are created due to successive fracture of particles under the increased loading stress (McDowell and Bolton, 1998). This process would result in more efficient granular packing and denser samples. Nakata et al. (1999) presented statistical data of particle breakage during the one-dimensional normal compression. They observed that once the vertical loading exceeds the yield stress, catastrophic particle splitting occurs in uniformly graded sample, while a distinctly different particle breakage pattern of asperity damage and surface grinding dominates in well-graded sands. The difference may originate from the high packing efficiency of well-graded sample in which the coarse particles normally have high coordination number, resulting in low probability of breakage (Wood, 2008). This finding is supported by a detailed discrete element analysis of isotropic compression on crushable aggregates in Bolton et al. (2008) that for uniformly graded soil samples, the particle breakage starts with the asperity damage under low loading stress, and then transforms to particle-splitting when the yielding stress is approached. At higher loading stress, both types of particle breakage exist for all grains. Based on a series of one-dimensional normal compression tests, Cil and Alshibli (2014) concluded that particle breakages concentrate mainly close to the loading platen where the strong force chains dominate. A constant grading can finally be reached when the contact stresses between particles are too low to induce any further particle breakage (Coop et al., 2004). Altuhafi and Coop (2011) investigated the influence of initial particle grading and density on the mechanical responses of soil using small-scale oedometer cells (cell diameter = 20 mm and 38 mm). They

stated that a unique normal compression line can finally be reached after intense particle breakages during compression. The amount of particle breakage can be reduced, while significant plastic volumetric deformation still exists when the initial sample grading changes from uniformly graded to well-graded. The fine particles are generally less spherical, less convex and more elongated than the original particles.

To quantify particle morphological characteristics, a set of shape descriptors have been defined at different length scales, such as sphericity, roundness, convexity, aspect ratio, flatness and fractal dimension (Altuhafi et al., 2013, Blott and Pye, 2008, Yang and Luo, 2015, Zhou et al., 2015). Zhou et al. (2018) analysed the particle morphological features by the X-ray micro-computed tomography (μ CT) and spherical harmonic analysis. Based on the reconstructed 3D particle surface, they defined the shape descriptors as 3D sphericity, roundness and fractal dimension to quantify the global form, local features and surface textures. These descriptors have certain correlations with each other, depending on the distance between the characteristic scales. However, the μ CT test can hardly be used to analyse a large number of particles with various sizes due to the difficulty of sample preparation. Alternatively, image-based method by dynamic image analysis of the 2D particle projections has been introduced as a pragmatic approach for quantitative shape analysis. The surface textures and roughness features can thus be described by various methods, such as material roughness indices (Alshibli et al., 2015), statistical indices (Zheng and Hryciw, 2015) and Fourier descriptors (Mollon and Zhao, 2013). Altuhafi et al. (2013) compiled a database of particle shape descriptors for 36 different types of sands and developed empirical relationships between particle convexity and sphericity. They found that the angular particles normally have very rough surface (i.e. low convexity), whereas the rounded particles are relatively smooth (i.e. high convexity). This database was further employed in correlating the particle shape and the mechanical behaviour of natural sands by Altuhafi et al. (2016). By investigating particle breakage during ring shear tests, Zhang et al. (2017) found that coarse particles become smoother and less elongated due to splitting and abrasion, while the newly produced fine particles are generally angular with irregular shapes.

Although advancements exist, a comprehensive analysis of particle breakage and morphology variation for individual particles involved in tests is still necessary. Hence, this study devotes to bridge the gap between the macroscopic soil mechanical behaviour and the microscale particle characteristics. This paper presents the results of particle breakage and surface texture changes during one-dimensional normal compression tests on calcareous sands

with distinct initial particle shape mixtures. The particle shape descriptors are quantified for each individual particle in soil samples by dynamic image analysis. The remained paper is organized as follows: first, the testing methodology are given. Then, the analyses of experimental data are presented, with respect to the compressive behaviour of sands, characteristics of particle breakage and variation of shape morphology. The subsequent section discusses the correlations between different shape descriptors and significance of this study. The final section summarizes the major conclusions reached in this study.

Methodology

One-dimensional normal compression test

The current study investigates the mechanical response and the corresponding variation of particle morphology of calcareous sands during the one-dimensional normal compression tests. The testing materials are mainly carbonate sediments with high angularity, brittleness, porosity and weak cementation. The sand specimens are sampled from Yongshu Coral Reef, South China Sea (Wang et al., 2011). To remove the adverse impacts of impurities on the tests, before tests, the calcareous sands are washed by distilled water for several times and then dried in an oven. For consistency and detailed shape analysis, only particles of sizes ranging from 10 mm to 20 mm are randomly selected for the current study. The uniform gradation of selected sands is very narrow comparing to the field gradations, which only represents the general particle morphology of coarse calcareous sands.

As shown in Figure 1, the one-dimensional normal compression of sand sample is achieved by moving the vertical loading frame downwards to compress an oedometer. The calcareous sands are loaded in a cylindrical sample container with the inner diameter of 230 mm and height of 155 mm. The calcareous particles have very diverse shapes, such as blocky, flaky, branched and rodlike, in which the blocky particles have dominantly larger amount than the others in the field. For a rough classification, the calcareous sands are initially divided into four groups based on their shapes (see Figure 1). Then, various samples are prepared by mixing the blocky sands with other shaped particles (e.g. tests T1-T10), as shown in **Error! Reference source not found..** The morphological characteristics of individual particles before and after the compressions are measured by the dynamic image analysis. In this approach, the general mechanical behaviour of calcareous sands and the influence of particle morphology on soil behaviour can be analysed.

The sample is prepared by pouring 3482 g calcareous sands into the sample container and then compressing the sands slowly to the aimed height (h_0) of 95 mm. The initial bulk density (ρ) and void ratio (e_0) of the sample can thus be calculated as 0.87 g/cm³ and 2.195, respectively. A thin layer of Vaseline is applied on the inner surface of the sample container to reduce the side wall friction effect. The vertical loading and unloading stress paths follow 0 kPa, 50 kPa, 100 kPa, 200 kPa, 400 kPa, 800 kPa, 400 kPa, 200 kPa, 100 kPa, 50 kPa, 0 kPa, with each stress level being maintained for 1 hour. Since the materials are dry and highly brittle, it is assumed that the sample consolidation can complete fully during this period of time. Based on the dynamic image analysis, the initial sample consists of around 3000 coarse particles, while the after the compression it consists of around 15000 particles (excluding very fine sand powders of sizes smaller than 0.1 mm).

Dynamic image analysis

The Microtrac PartAn^{3D} Maxi Large particle size and shape analyser (Microtrac, 2018) (see Figure 2 (a)) has been employed for dynamic image analysis (DIA) to study the morphological parameters of each individual particle, such as size (e.g. length, width, thickness), form (e.g. sphericity, roundness, aspect ratio), surface roughness (e.g. convexity, concavity) and other (e.g. curvature). The system can characterize more than 30 morphological parameters of granular materials. It provides non-contact measurement of dry particles ranging in size from 0.16 to 135 μ m. It uses high-speed and high-resolution camera to take multiple images of each particle at different spatial locations and orientations. These images are then digitized and analysed by the PartAn^{3D} software to measure the particle length, width, thickness, perimeter and area, based on which the morphological parameters of each particle can be calculated. The system is able to analyse 100 images per second. The measurement principle complies with ISO 13322-2 for dynamic image analysis (ISO, 2006).

As shown in Figure 2 (b), the dry particle sample is first placed in the funnel on the top left. Then, they are released to move along the vibratory feeder to the edge of the sensing zone, where they fall by gravity through the sensing zone and collected by the sample box at the bottom. The light strobe on one side of the sensing zone lights the particles and the digital camera on the other side photographs the particles as they tumble through the sensing zone. The vibrations of particles in the vibratory feeder allow them to fall with rotational speed, such that different orientations of particles can be captured by the high-speed camera in the sensing zone. A video file of the testing and analysing process is automatically recorded, which can be

reloaded and analysed for later use. The particle distribution and summary of morphological parameters for each particle are then calculated and reported by the data analysis system.

Measurement principle and particle shape descriptors

The PartAn^{3D} particle tracking system enables the high-speed camera to take multiple photos of individual particles when they tumble randomly through the sensing zone, as shown in Figure 3. These photos are then digitized to compute the morphological parameters based on the known size and location of the pixels in each image (see Figure 4). The Feret size has been measured as the distance between two parallel planes restricting the object perpendicular to the planes. The largest Feret size (F_{\max}) measured in a series of individual particle images are assigned as the 3D length (FL), while the smallest Feret size (F_{\min}) is assigned as the thickness (FT) of that particle. The maximum value of F_{\min} in a series of measurements is denoted as the width (FW) of the same particle. The particle area (A) is calculated by counting the pixels covered by the particle image and using the size of the pixel. Based on these measured parameters, a set of key shape descriptors can be defined as follows:

$$\text{Equivalent diameter} \quad D = \sqrt{4A/\pi} \quad (1)$$

$$\text{Aspect ratio} \quad \alpha = FW/FL \quad (2)$$

$$\text{Flatness} \quad \beta = FT/FW \quad (3)$$

$$\text{Roundness} \quad R = 4A/\pi FL^2 \quad (4)$$

$$\text{Sphericity} \quad S = 4\pi A/P_p^2 \quad (5)$$

$$\text{Convexity} \quad C = P_c/P_p \quad (6)$$

Among these parameters, D quantifies the diameter of equivalent circle with the same area as the particle; α , β , R and S are particle form parameters quantifying particle shape; C describes particle surface roughness. Physically, particles with small aspect ratio, flatness and convexity are generally elongated, flat and rough. The higher the values of R and S , the particle profile is more rounded and closer to a sphere. Since roundness is scale dependent, it is typically described qualitatively (Altuhafi et al., 2013). Thus, instead of roundness, the current study uses sphericity (S) as the fundamental shape descriptor to represent particle form.

Results

The influence of particle shape on soil compression

To investigate the influence of particle shape on the mechanical response of calcareous sands, samples of various particle shape mixtures have been tested in the one-dimensional normal compression. The variations of void ratio with the vertical loading stress are shown in Figure 5. In the analyses, the void ratio of the sample during the compression is computed as:

$$e = e_0 - (1 + e_0) \Delta h / h_0 \quad (7)$$

where e_0 and h_0 are the initial sample void ratio and height; Δh is the vertical displacement of the loading frame.

According to Figure 5, at low loading stresses ($\sigma_v \leq 100$ kPa), the void ratios of different samples decrease very slowly due to the high resistance from the internal friction and interlocking of particles. As the vertical loading stress increases and gradually exceeds the particle resistant strength ($\sigma_v > 200$ kPa), the void ratios of different calcareous samples decrease rapidly. At the peak loading stress ($\sigma_v = 800$ kPa), sample T1 (i.e. blocky particles) exhibits the lowest void ratio among all the tests, indicating that the blocky particles can be packed denser than the irregular particles. For tests with the same type of particle shape mixture, samples of medium percentage of mixed irregular particles (20%) exhibit the highest void ratio during the loading and unloading stage (e.g. T3, T6 and T9). In particular, T9 has the highest void ratio among all the tests. The results are as expected, because the void ratio of granular packing increases as the particle aspect ratio decreases (Meng et al., 2012). However, intense particle breakages can occur for samples of higher percentage of mixed irregular particles (e.g. 30%), which would decrease the void ratio of the sample significantly. Thus, samples consisting of more elongated rodlike particles (i.e. T9 and T10) normally have high void ratios at very loose packing states. Apparent oscillations of void ratios can also be observed during the loading stage on the curves when the vertical loading stress changes at each loading step. During the unloading stage, the void ratio increases very little (< 0.05), indicating that the sample deformation is mainly due to particle breakage which cannot be recovered when the vertical loading stress is released. Though the exact normal compression lines (NCL) of these tests are different, they have the same inclination (i.e. the same compression index, C_c).

Particle breakage

The particle breakage can be qualitatively analysed by comparing the particle size distribution (PSD) curves before and after the compression test. The traditional sieve analysis uses a nest of sieves with various sized square or circular openings to measure the mass distribution by size of granular samples. This approach actually measures the middle dimension of individual particles, i.e. width, while the smallest and largest dimensions cannot be captured as particles can always pass the sieve at appropriate orientations. The sieve analysis only quantifies the characteristics of particle size distribution in several distinct size ranges, while no grading information can be extracted between the size intervals. The sieve analysis is always time consuming, e.g. more than 30 minutes for a standard test. Alternatively, the PSD of particles can be quantified by the dynamic image analysis on the scanning data from the Microtrac PartAn^{3D} Maxi Large particle size and shape analyser. It has apparent advantages when compared with the traditional sieve analysis, as it directly measures the size and volume of each individual particle in the sample. If the density is given, the particle mass can be readily obtained. This approach can greatly improve the overall resolution and accuracy of particle size characterization. The measurement can be done automatically within two minutes. The current study calculates the particle size distribution based on the volume of individual particles, so that the measurement is in accordance with the results by sieve analysis.

For ease of comparison, only results of tests T1, T4, T7 and T10 have been reported in this study. As shown in Figure 6, before compression, the sample of pure blocky particles is uniformly graded with particle size in the range of 10 mm – 20 mm. The addition of 30% irregular particles (i.e. flaky, branched and rodlike) transforms the PSD curve slopes to become gentler, indicating that the proportion of coarse grains becomes higher than the blocky sample. In particular, the mixture of rodlike particles has the gentlest grading curve, showing apparent increase of coarse grains in the sample. After the compression, the sample grading curves shift to the fine size range as well-graded (see the arrow on the figure), because a large number of fine grains have been produced due to particle breakage. This effect will lead to more efficiently packed dense samples. In this study, the final particle size varies widely from 2 mm to 20 mm. The mixture of rodlike particles remains to be the coarsest grading, while the flaky and branched mixtures have almost the same intermediate particle size grading.

A quantitative analysis using particle breakage factor (B_p) can be performed based on the change of particle surface area during the test. In dynamic image analysis, the change of particle surface area is measured by the change of perimeters as an alternative approach for two-

dimensional analysis, as

$$B_r = \frac{1}{2}(\sum P - \sum P_0) / \sum P_0 \quad (8)$$

where $\sum P_0$ and $\sum P$ are the total particle perimeters before and after the test, respectively.

Error! Reference source not found. summarizes the results of particle breakage factor (B_r) for tests of various particle shape mixtures and contents. According to the table, an abrupt change of particle breakage occurs when the mixture content increases from 0% to 10%. Though no clear dependence of mixture content and B_r can be formulated, the general trend shows that the mixture of branched particles in blocky sands can increase the particle breakage. This is as expected because the structure of branched particles can be easily crushed during compression due to stress localization. For mixture of rodlike particles, B_r first increases and then decreases with the mixture content. This indicates that the blocky particles can be crushed more effectively when a small amount of rodlike particles are mixed in the sample. At higher mixture content, the value of B_r is very low because less blocky particles can be crushed and the rodlike particles can effectively resist compression induced breakage. In this study, the values of B_r obtained from dynamic image analysis can match well the typical range of particle breakage factors (0.2-0.55) calculated from particle size distribution curves (Wei et al., 2018), indicating that Eq.(8) can effectively quantify particle breakages. As stated in Bolton et al. (2008), particle breakage is initiated by asperity damage, which is followed by grain-splitting when soil starts to yield. In fact, damages by splitting have been widely observed for coarse particles under loading. Figure 7 shows that the brittle damage of particles occurs preferentially in the middle of the particle. Though large particles have relatively low tensile strength, the high coordination numbers with the surrounding fine grain contacts make them less likely to be crushed (e.g. the rodlike particles) (McDowell and Bolton, 1998).

The breakage of particles, either by asperity damage or splitting, can produce a huge number of fine particles. This is directly illustrated by the increase of fine particle distribution frequency in the granular sample. In the statistical analysis, particles smaller than 1 mm are ignored, because they only amount to less than 0.1% of the total mass (see Figure 6). As shown in Figure 8, before the compression, the particle size distributes dominantly (> 70%) in the range of 9 – 12 mm, following the Gaussian distribution pattern. Since the equivalent diameter (D) is used, the lower bound of particle size is slightly smaller than the minimum size obtained from sieve analysis (i.e. 10 mm). After the compression, the majority of particles (> 70%) have

the size smaller than 5 mm, indicating that coarse particles have been crushed to produce a huge number of fine particles. The distribution pattern also transforms from Gaussian to exponential distributions. For various tests, the initial uniformly distributed blocky particles (i.e. T1) are crushed more thoroughly with more fine particles. This shows that the force transmission at particle contacts in the densely packed sample can be well maintained and uniformly distributed, which cause efficient particle asperity damage. On the other hand, the breakage of branched and rodlike particles (i.e. T7 and T10) can still retain relatively high portion of coarse particles ($D > 8$ mm), because the splitting of elongated particles will increase the number of coarse particles of similar sizes. However, this damage pattern is far less frequent than the asperity damage during the compression. Thus, the increase of coarse particle frequency is less evident than that of fine particles.

Change of particle shape descriptors

The particle shape descriptors are analysed before and after the compression tests, such that the change of particle morphology under loading can be illustrated. Figure 9 shows the statistical results of particle shape descriptors for soil sample consisting of purely blocky sand particles. Before the compression, the shape factor frequency follows well the Gaussian distribution. After the compression, the frequency of particle sphericity, aspect ratio and flatness can still follow the Gaussian distribution, except for the particle convexity that a large portion of particles have high convexity values (i.e. smooth surface). According to Figure 9 (a), the particle sphericity decreases slightly after the compression, illustrating that more angular particles have been produced by splitting and abrasion. The particle convexity increases towards the unity value (Figure 9 (b)), meaning that the particle surface has become smoother due to asperity damage. Figure 9 (c) shows that the mean particle aspect ratio decreases slightly, indicating that more elongated particles have been produced after the compression. In addition, a large number of very flat particles (i.e. low flatness) are also produced (Figure 9 (d)). The characteristics of particle shape descriptor distribution illustrate that the breakage of blocky calcareous particles by splitting makes the particles to become more elongated and flatter, while the asperity damage can increase the particle surface smoothness.

Figure 10 illustrates the variation of mean particle shape descriptors before and after the compression for tests of different particle shape mixtures (e.g. flaky, branched and rodlike). In the initial sample, as the content of particle mixture increases, the mean particle sphericity decreases approximately linearly, as shown in Figure 10 (a). This is as expected because the

mixed particles are highly irregular. Different samples exhibit very close sphericity values because of the dominantly high percentage of blocky particles (>70%). After the compression, the mean sphericity of particle mixtures increases slightly due to particle breakage (mainly by asperity abrasion damage). Figure 10 (b) shows that before compression, as the mixture content increases, the mean particle convexity remains almost constant for the flaky and rodlike particle mixtures, while it decreases slightly for branched particle mixture as particle surface becomes rougher. After the compression, the mean particle convexity increases slightly with the mixture percentage for different samples when compared to the initial value. This is mainly due to the asperity damage of individual particles, which polishes the particle surface to be smoother. Figure 10 (c) shows that before compression, the mean particle aspect ratio decreases with the percentage of particle mixture. In particular, the rodlike particle mixture has the smallest aspect ratio due mainly to the increase of elongated particles in the sample. After compression, the mean particle aspect ratio decreases slightly and tends to be constant, because the particle breakage by splitting can reduce the overall particle aspect ratio (see the illustration in Figure 7). Figure 10 (d) shows that before compression, the branched and rodlike mixture samples have almost constant flatness values as the percentage of mixture increases. However, for the flaky mixture, the flatness decreases quickly following a linear relationship. This is as expected because the flaky particles have very flat profile. After the compression, the mean particle flatness values of different tests all decrease, indicating that particles become flatter due to breakage. The branched and rodlike mixtures have particularly significant reductions of flatness, because the coarse particles have been crushed to be finer in size.

Figure 11 illustrates the mean particle shape descriptors for particles of various sizes before and after the compression tests. In the analyses, the mean particle shape descriptor is computed by averaging the values of all particles with the corresponding equivalent diameter within each 1 mm interval. Results for particles of equivalent diameter larger than 20 mm are not reported here due to the limited small number of particles for statistical purpose. As shown in Figure 11 (a), for test of purely blocky particles, the particle aspect ratio and flatness increase with D , while the sphericity and convexity remains almost constant. The results indicate that the fine particles tend to be more elongated and flatter than the coarser ones. However, their sphericity and convexity change little and remain as relatively high values, showing that the particles are rounded and smooth. Figure 11 (b) shows that there is a rapid increase of particle flatness with diameter for the sample mixed with 30% flaky particles (T4). This indicates that coarse particles (mainly blocky particles) tend to be relative thicker than the finer ones (mainly flaky

particles). The mean particle flatness increases by about 0.05 after the compression, due mainly to the reduction of particle width via asperity damage and splitting. The mean particle sphericity, convexity and aspect ratio change little after the compression, remaining almost constant for different sized particles. Figure 11 (c) illustrates that for the branched mixture sample, before compression, the mean particle aspect ratio decreases, while the mean particle flatness increases with the equivalent particle diameter. The mean particle sphericity and convexity values are almost constant for different particle sizes. After the compression, all these shape descriptors increase slightly for the corresponding particle sizes. The produced fine particles are more rounded, smoother and less elongated (i.e. higher sphericity, convexity and aspect ratio), but flatter (i.e. lower flatness) than the coarser particles. The results indicate that the branched particles of large projected sizes are normally elongated and thick, with relatively rounded and smooth surface. The breakage of these branched particles would produce many flatter and smoother fine particles. Figure 11 (d) shows that for the rodlike mixture sample, before compression, the mean particle aspect ratio decreases, while the flatness increases rapidly with the equivalent particle diameter. The mean particle sphericity and convexity remain constant for various sized particles. After the compression, these shape descriptors change little for the corresponding particle sizes, while the produced fine particles are more spherical, smoother, less elongated and flatter than the coarser ones. This is as expected because the breakage of coarse rodlike particles (mainly by splitting, see Figure 7 (d)) would produce many short rodlike particles, changing significantly the particle aspect ratio and flatness. The decrease of flatness for fine particles is due mainly to the breakage of the blocky particles which has the dominantly high mass percentage (70%) in the sample.

Discussion

In the analysis, it is difficult to establish simple correlations between different shape descriptors due to the wide scattering of data distributions. This has also been noted in Altuhafi et al. (2013). The most consistent trend in data distribution is the correlation between particle sphericity and convexity, as shown in Figure 12. The results of this study are distributed within two limiting lines (the black solid lines), while most of the data are concentrated within the two red dashed lines. The general trend illustrates the increase of particle sphericity with convexity, indicating that the rounded (spherical) particles tend to be smoother than the angular ones. According to the particle shape classification system in Altuhafi et al. (2013), particles evolve gradually from very angular, angular, subangular, subrounded, rounded, to well-rounded for data points distributed from the bottom left to the upper right zones in Figure 12. The rounded

particles generally have very high values of both convexity and sphericity, while angular particles have low combinations of these two descriptors. The current results on calcareous sands can partly match well the data in Altuhafi et al. (2013) (mainly coarse quartz sands) for particle convexity higher than 0.95, while large discrepancy still exists for particles with lower convexity. The difference may result from the unique features of calcareous sands with high brittleness, porosity and angularity that the rough asperity can be easily polished during compression.

In this study, calcareous sand samples of a certain amount of rodlike particles exhibit relatively high void ratio and low breakage factor. This feature leads to a relatively low compressibility of the sand sample. Thus, engineering compaction work on these sands would normally require high compacting effort to achieve the aimed soil density. Once it is fully compacted, the induced particle breakage can facilitate the consolidation of soil. In particular, the fine grains can effectively fill up the voids between the coarse grains, which act as the cushion layer to prevent further particle breakage. This is highly beneficial for engineering construction with high soil compactness and strength, so that small post-consolidation ground deformation can be achieved.

Conclusions

This research has attempted to quantify the morphology of individual particles involved in the one-dimensional compression test by using the dynamic image analysis. The results presented in this paper clarify some important aspects of soil compaction and particle breakage for calcareous sands. First, the compression of different particle mixtures would result in normal compression lines of the same inclination due to particle breakage at all scales. The mixture of branched particles in blocky sands can effectively increase the particle breakage factor because of the highly brittle branched structure. The produced fine particles follow well exponential frequency distributions (by number). These huge number of fine particles can effectively fill up the voids between coarse particles, increasing the overall packing efficiency and strength of calcareous sands. In addition, the coarse particles can be cushioned by the fines, so that their breakage potential in the subsequent compression is reduced.

The results also show that the distribution frequency of particle shape descriptors before and after the compression all follow well the Gaussian distribution pattern (except the convexity after the test). The fine particles are normally more elongated and flatter than the coarse ones. After the compression tests, all particles tend to be slightly smoother and more

spherical than the original sample, due mainly to the particle asperity damage. In particular, the rounded (spherical) particles are much smoother than the angular ones. The variation of particle morphology indicates that the compression of calcareous sands can make the particles smoother and more rounded, which can improve the overall soil performance in subsequent engineering work.

Data Availability Statement

All data generated during the study are available from the corresponding author by request.

Acknowledgements

This research was supported by the Strategic Priority Research Program of the Chinese Academy of Sciences (grant XDA19060301 and grant XDA13010200), the National Natural Science Foundation of China (grant 41877260, 41877267 and 41602289). All these supports are acknowledged.

References

- Alshibli, K. A., Druckrey, A. M., Al-Raoush, R. I., Weiskittel, T., and Lavrik, N. V. (2015). "Quantifying Morphology of Sands Using 3D Imaging." *Journal of Materials in Civil Engineering*, 27(10), 04014275.
- Altuhafi, F., O'Sullivan, C., and Cavarretta, I. (2013). "Analysis of an Image-Based Method to Quantify the Size and Shape of Sand Particles." *J. Geotech. Geoenviron.*, 139(8), 1290-1307.
- Altuhafi, F. N., and Coop, M. R. (2011). "Changes to particle characteristics associated with the compression of sands." *Géotechnique*, 61(6), 459-471.
- Altuhafi, F. N., Coop, M. R., and Georgiannou, V. N. (2016). "Effect of Particle Shape on the Mechanical Behavior of Natural Sands." *J. Geotech. Geoenviron.*, 142(12), 04016071.
- Blott, S. J., and Pye, K. (2008). "Particle shape: a review and new methods of characterization and classification." *Sedimentology*, 55(1), 31-63.
- Bolton, M. D., Nakata, Y., and Cheng, Y. P. (2008). "Micro- and macro-mechanical behaviour of DEM crushable materials." *Géotechnique*, 58(6), 471-480.
- Cavarretta, I., O'Sullivan, C., and Coop, M. R. (2017). "The relevance of roundness to the crushing strength of granular materials." *Géotechnique*, 67(4), 301-312.
- Chen, Q., Indraratna, B., Carter, J. P., and Nimbalkar, S. (2015). "Isotropic-kinematic hardening model for coarse granular soils capturing particle breakage and cyclic loading under triaxial stress space." *Canadian Geotechnical Journal*, 53(4), 646-658.
- Cheng, Y. P., Bolton, M. D., and Nakata, Y. (2004). "Crushing and plastic deformation of soils simulated using DEM." *Géotechnique*, 54(2), 131-141.
- Cil, M. B., and Alshibli, K. A. (2014). "3D evolution of sand fracture under 1D compression." *Géotechnique*, 64(5), 351-364.

- Coop, M. R., and Lee, I. K. "The behaviour of granular soils at elevated stresses." *Proc., Predictive soil mechanics*, Thomas Telford, London, 186-198.
- Coop, M. R., Sorensen, K. K., Freitas, T. B., and Georgoutsos, G. (2004). "Particle breakage during shearing of a carbonate sand." *Géotechnique*, 54(3), 157-163.
- Ghafghazi, M., Shuttle, D. A., and DeJong, J. T. (2014). "Particle breakage and the critical state of sand." *Soils and Foundations*, 54(3), 451-461.
- Hardin, B. O. (1985). "Crushing of Soil Particles." *Journal of Geotechnical Engineering*, 111(10), 1177-1192.
- Hyodo, M., Hyde, A. F. L., Aramaki, N., and Nakata, Y. (2002). "Undrained monotonic and cyclic shear behaviour of sand under low and high confining stresses." *Soils and Foundations*, 42(3), 63-76.
- ISO (2006). "Image analysis methods - Part 2: Dynamic image analysis methods." *Particle size analysis*, International Organization for Standardization, Switzerland.
- Kikumoto, M., Wood, D. M., and Russell, A. (2010). "Particle crushing and deformation behaviour." *Soils and Foundations*, 50(4), 547-563.
- Lade, P., Yamamuro, J., and Bopp, P. (1996). "Significance of Particle Crushing in Granular Materials." *Journal of Geotechnical Engineering*, 122(4), 309-316.
- McDowell, G. R., and Bolton, M. D. (1998). "On the micro-mechanics of crushable aggregates." *Géotechnique*, 48(5), 667-679.
- Meng, L., Lu, P., Li, S., Zhao, J., and Li, T. (2012). "Shape and size effects on the packing density of binary spherocylinders." *Powder Technology*, 228, 284-294.
- Microtrac (2018). "PartAn 3-D Maxi Large particle size and shape analyser." <<https://www.microtrac.com/eur/partan-3-d-maxi-large-particle-size-and-shape-analyzer/>>.
- Mollon, G., and Zhao, J. (2013). "Generating realistic 3D sand particles using Fourier descriptors." *Granular Matter*, 15(1), 95-108.
- Nakata, A. F. L., Hyde, M., Hyodo, H., and Murata (1999). "A probabilistic approach to sand particle crushing in the triaxial test." *Géotechnique*, 49(5), 567-583.
- Wang, X. Z., Jiao, Y. Y., Wang, R., Hu, M. J., Meng, Q. S., and Tan, F. Y. (2011). "Engineering characteristics of the calcareous sand in Nansha Islands, South China Sea." *Engineering Geology*, 120(1-4), 40-47.
- Wei, H., Zhao, T., He, J., Meng, Q., and Wang, X. (2018). "Evolution of Particle Breakage for Calcareous Sands during Ring Shear Tests." *Int. J. Geomech.*, 18(2), 04017153.
- Wood, D. M., and Maeda, K. (2007). "Changing grading of soil: effect on critical states." *Acta Geotechnica*, 3(1), 3-14.
- Wood, M. D. "Critical state and soil modelling." *Proc., Deformational characteristics of geomaterial*, IOS Press, Amsterdam, The Netherlands, 51-72.
- Xiao, Y., and Liu, H. (2017). "Elastoplastic Constitutive Model for Rockfill Materials Considering Particle Breakage." *Int. J. Geomech.*, 17(1).
- Xiao, Y., Liu, H., Ding, X., Chen, Y., Jiang, J., and Zhang, W. (2016). "Influence of Particle Breakage on Critical State Line of Rockfill Material." *Int. J. Geomech.*, 16(1), 04015031.
- Xiao, Y., Long, L., Evans, T. M., Zhou, H., Liu, H., and Stuedlein, A. W. (2019). "Effect of Particle Shape on Stress-Dilatancy Responses of Medium-Dense Sands." *J. Geotech.*

- Geoenviron.*, 145(2), 04018105.
- Xiao, Y., Meng, M., Daouadji, A., Chen, Q., Wu, Z., and Jiang, X. (2018). "Effects of particle size on crushing and deformation behaviors of rockfill materials." *Geoscience Frontiers*.
- Xiao, Y., Wang, L., Jiang, X., Evans, T. M., Stuedlein, A. W., and Liu, H. (2019). "Acoustic Emission and Force Drop in Grain Crushing of Carbonate Sands." *J. Geotech. Geoenviron.*, 145(9), 04019057.
- Yang, J., and Luo, X. D. (2015). "Exploring the relationship between critical state and particle shape for granular materials." *J. Mech. Phys. Solids*, 84, 196-213.
- Zhang, X., Baudet, B. A., Hu, W., and Xu, Q. (2017). "Characterisation of the ultimate particle size distribution of uniform and gap-graded soils." *Soils and Foundations*, 57(4), 603-618.
- Zheng, J., and Hryciw, R. D. (2015). "Traditional soil particle sphericity, roundness and surface roughness by computational geometry." *Géotechnique*, 65(6), 494-506.
- Zhou, B., Wang, J., and Wang, H. (2018). "Three-dimensional sphericity, roundness and fractal dimension of sand particles." *Géotechnique*, 68(1), 18-30.
- Zhou, B., Wang, J., and Zhao, B. (2015). "Micromorphology characterization and reconstruction of sand particles using micro X-ray tomography and spherical harmonics." *Engineering Geology*, 184(Supplement C), 126-137.

Figure 1. One-dimensional normal compression of calcareous sand particles. The particle shapes from the top down are flaky, blocky, branched and rodlike, respectively.

Figure 2. (a) A photo of the PartAn^{3D} Maxi Large particle size and shape analyser; (b) a schematic view of the testing system.

Figure 3. Series of particle images during tumbling through the sensing zone for four typical particles. Each row of the figure shows the successive images of a specific particle.

Figure 4. Digitized particle image and definitions of maximum (F_{max}) and minimum (F_{min}) Feret sizes, equivalent circle, perimeter of the particle (P_p) and the convex hull perimeter (P_c), respectively. The convex hull perimeter can be visualised as the length of an elastic band placed around the particle.

Figure 5. One-dimensional compression plot for calcareous sand samples of various particle mixtures.

Figure 6. Initial (solid curve) and final (dashed curve) gradings of calcareous sand samples.

Figure 7. Selected photos of particle breakage after the compression. (a): blocky particle; (b): flaky particle; (c): branched particle; (d): rodlike particle.

Figure 8. The distribution frequency (by number) of particle size of various equivalent diameters before and after the compression test. (a): test of pure blocky particles (T1); (b): test of 70% blocky and 30% flaky particles (T4); (c): test of 70% blocky and 30% branched particles (T7); (d): test of 70% blocky and 30% rodlike particles (T10). In the analyses, particles of sizes smaller than 1 mm are ignored due to their low weight.

Figure 9. Distribution of particle shape descriptors before and after the compression test. (a): sphericity; (b): convexity; (c): aspect ratio; (d) flatness. The statistical data are fitted by Gauss distribution functions.

Figure 10. Variation of mean particle (a) sphericity, (b) convexity, (c) aspect ratio and (d) flatness. The solid symbols represent values before the compression, while the hollow symbols represent values after the compression. Data points corresponding to the mixture percentage of 0% are for pure blocky particles.

Figure 11. Mean particle shape descriptors for particles of various sizes before (solid symbols) and after (hollow symbols) the uniaxial compression tests. (a): test of pure blocky particles (T1); (b): test of 70% blocky and 30% flaky particles (T4); (c): test of 70% blocky and 30% branched particles (T7); (d): test of 70% blocky and 30% rodlike particles (T10).

Figure 12. Plot of sphericity against convexity for sands before and after the compression tests. The mean particle shape descriptors in Altuhafi et al. (2013) are also included for comparison purpose.

Table 1. Calcareous sand samples of various particle shape mixtures (weighted by mass percentage)

Particle shape	T1	T2	T3	T4	T5	T6	T7	T8	T9	T10
Blocky (%)	100	90	80	70	90	80	70	90	80	70
Flaky (%)	0	10	20	30	0	0	0	0	0	0
Branched (%)	0	0	0	0	10	20	30	0	0	0
Rodlike (%)	0	0	0	0	0	0	0	10	20	30

Table 2. Particle breakage coefficients for tests of various particle shape mixtures.

% mixture	Flaky	Branched	Rodlike
0	0.449	0.449	0.449
10%	0.373	0.382	0.466
20%	0.336	0.44	0.393
30%	0.402	0.455	0.384

Figure 1

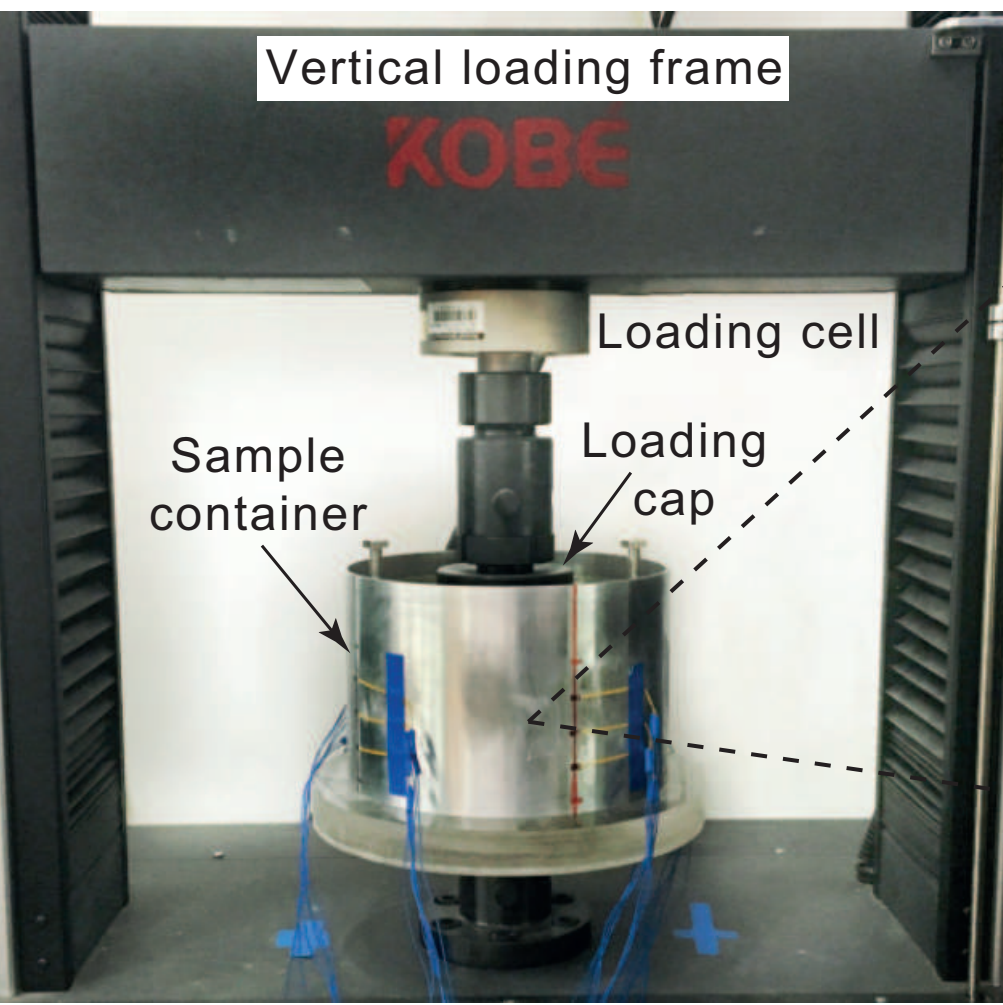


Figure 2
(a)



(b)

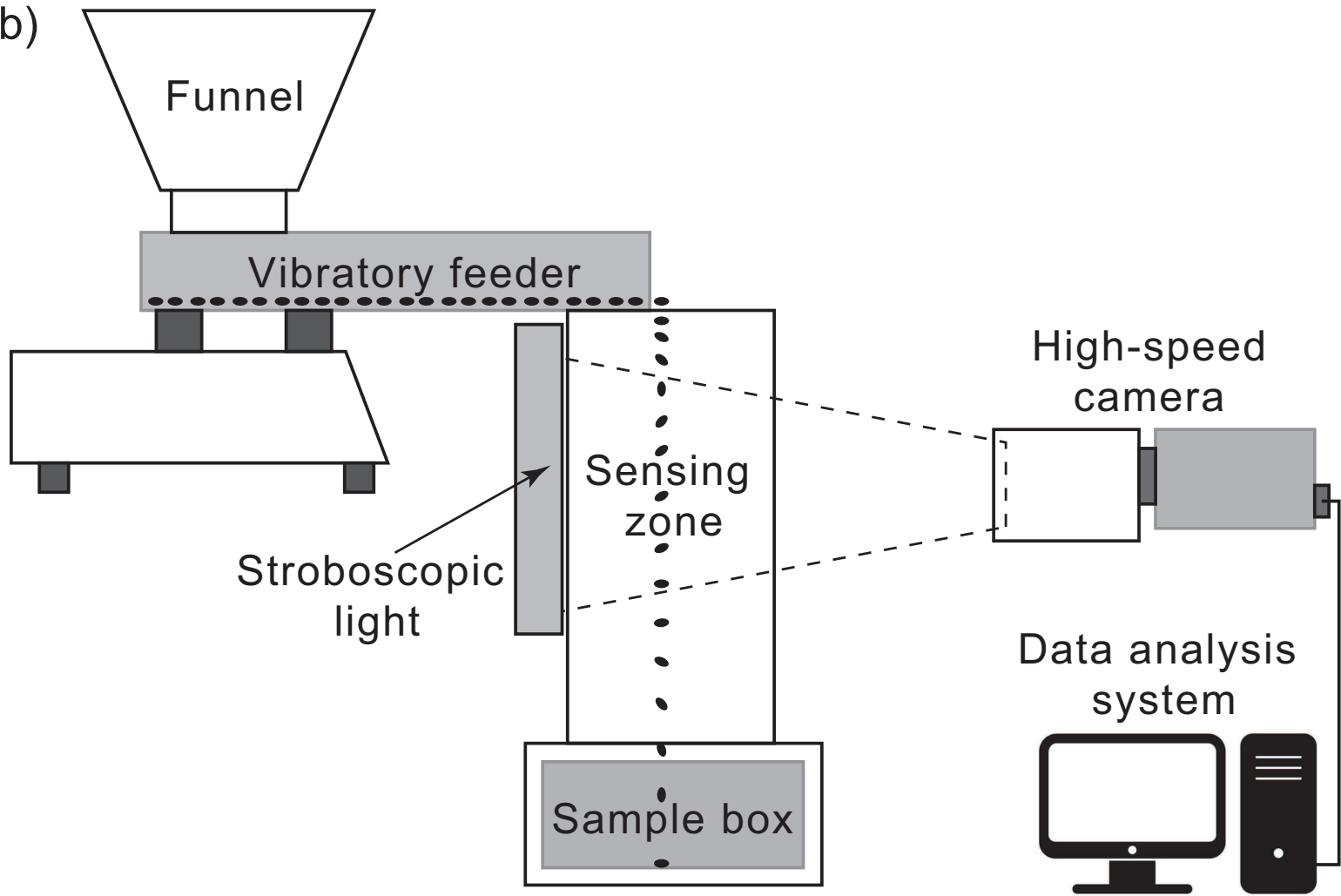


Figure 3

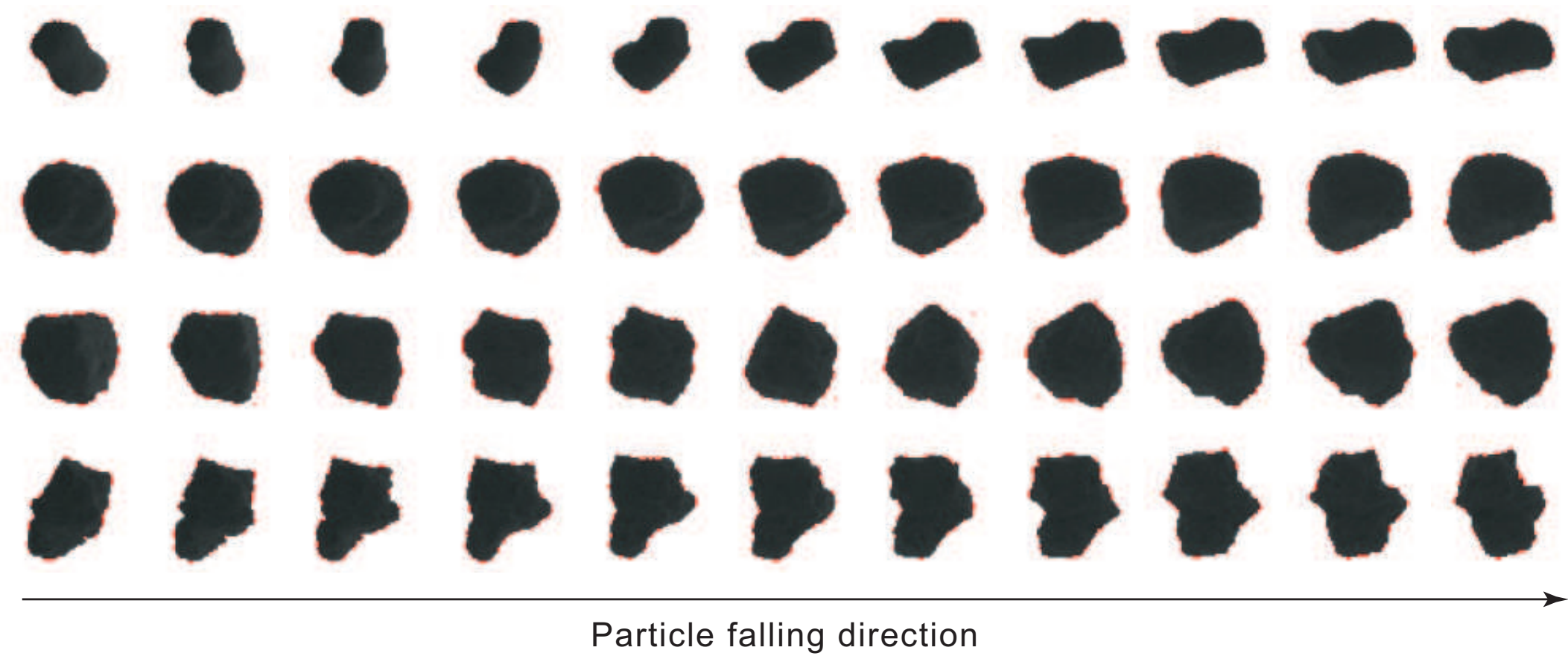


Figure 4

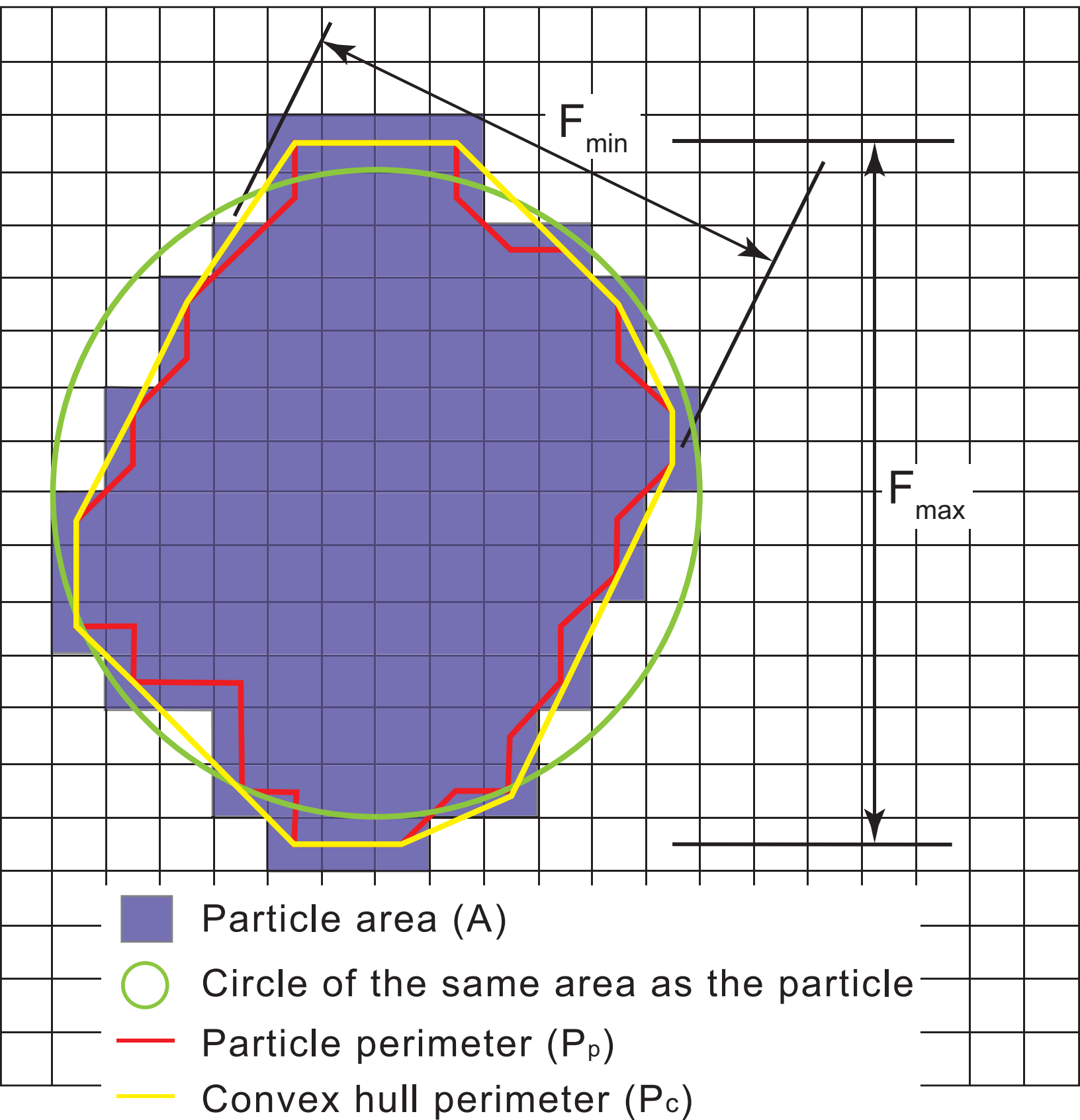
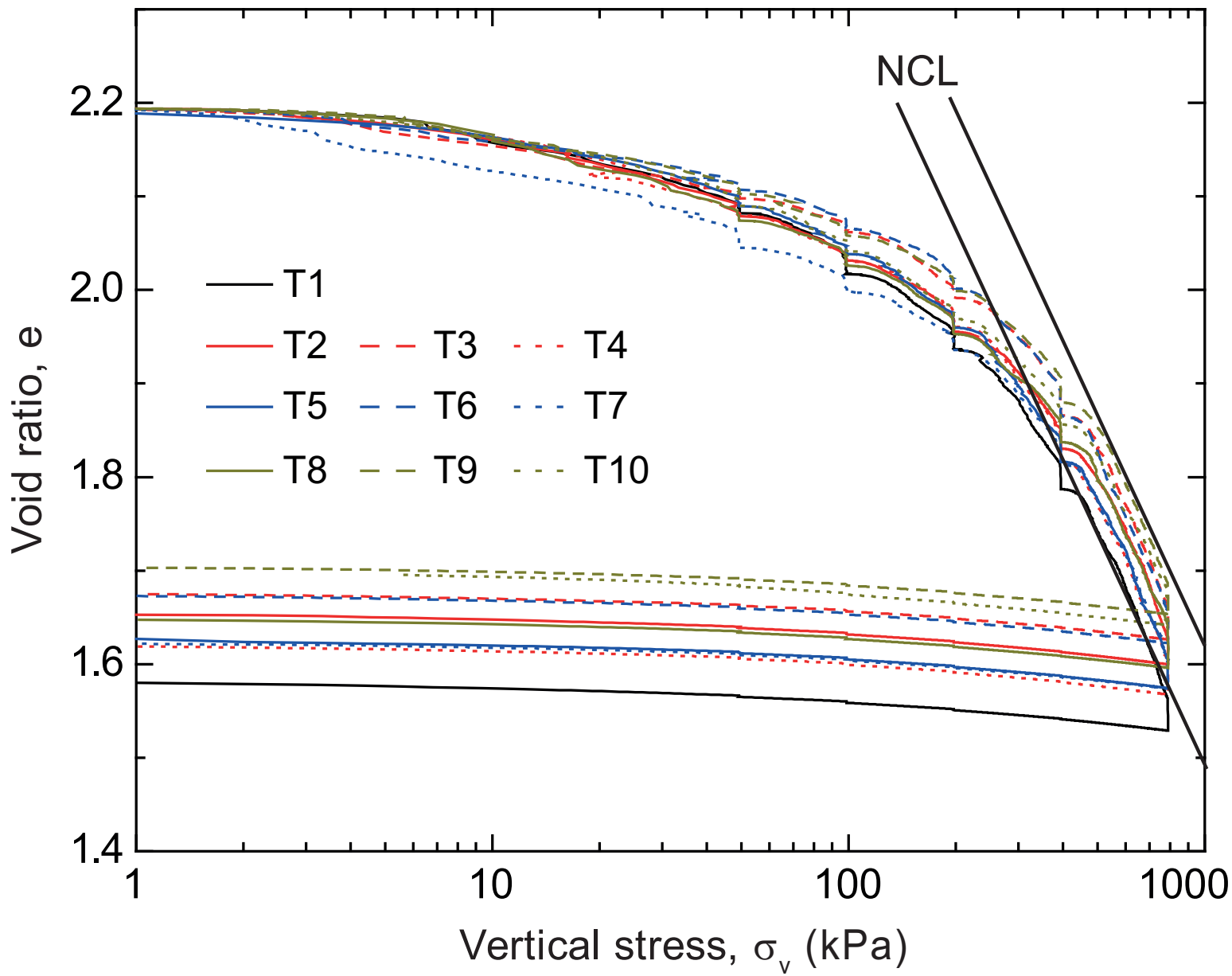


Figure 5



(a)



(b)



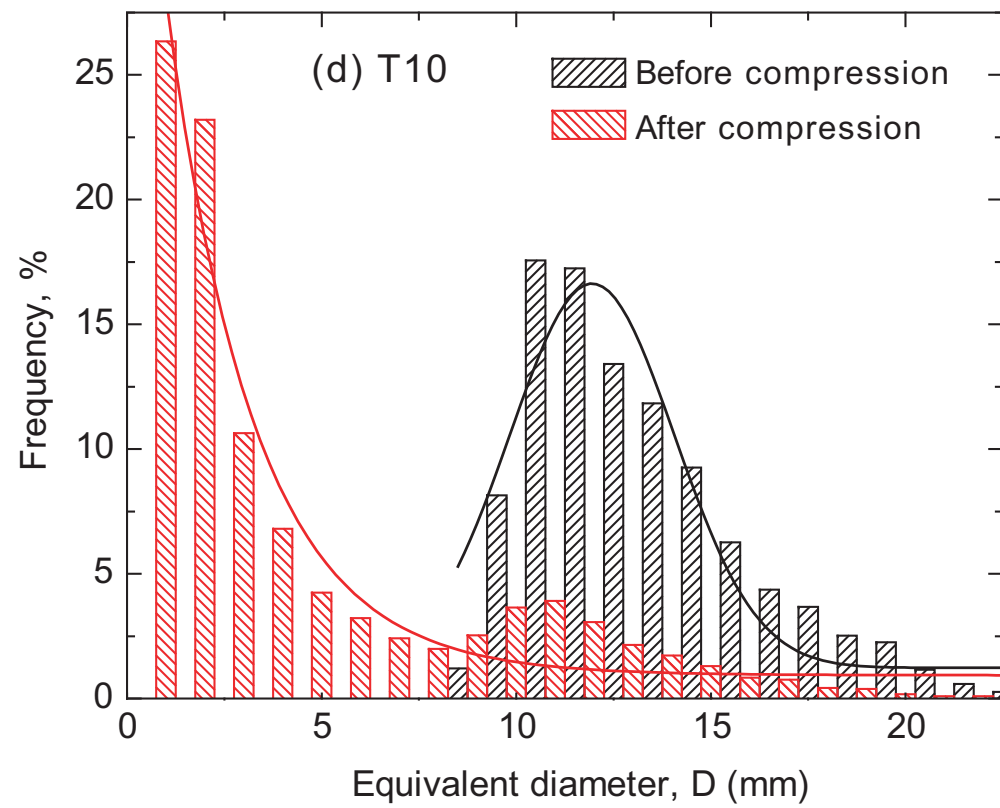
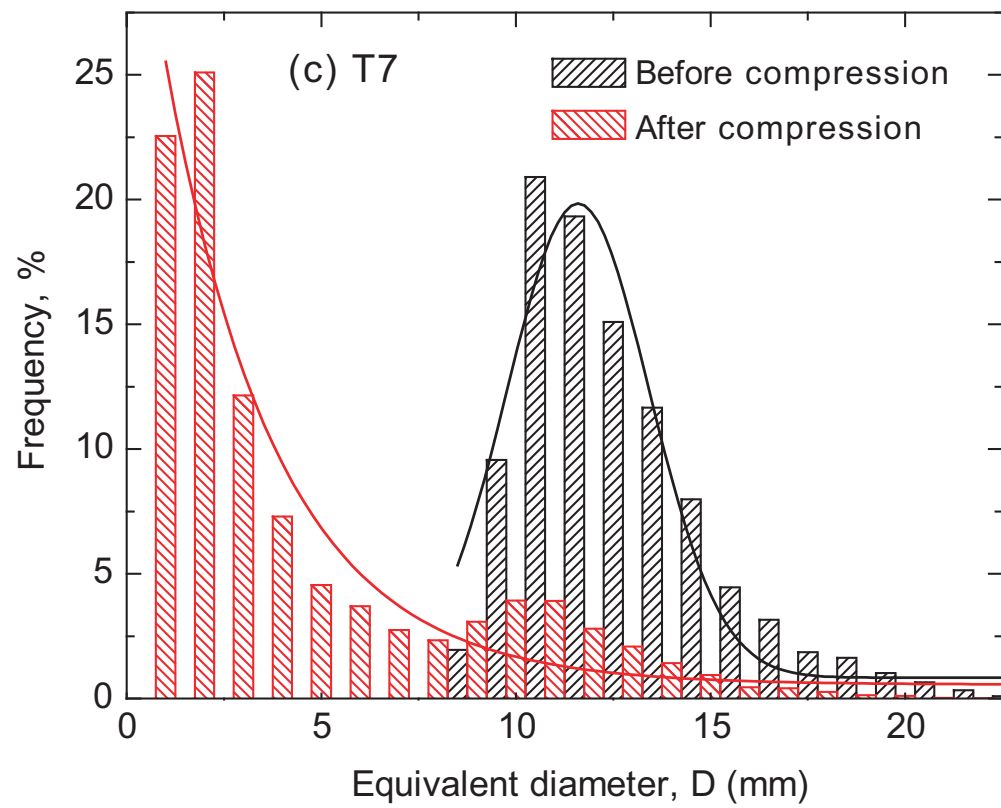
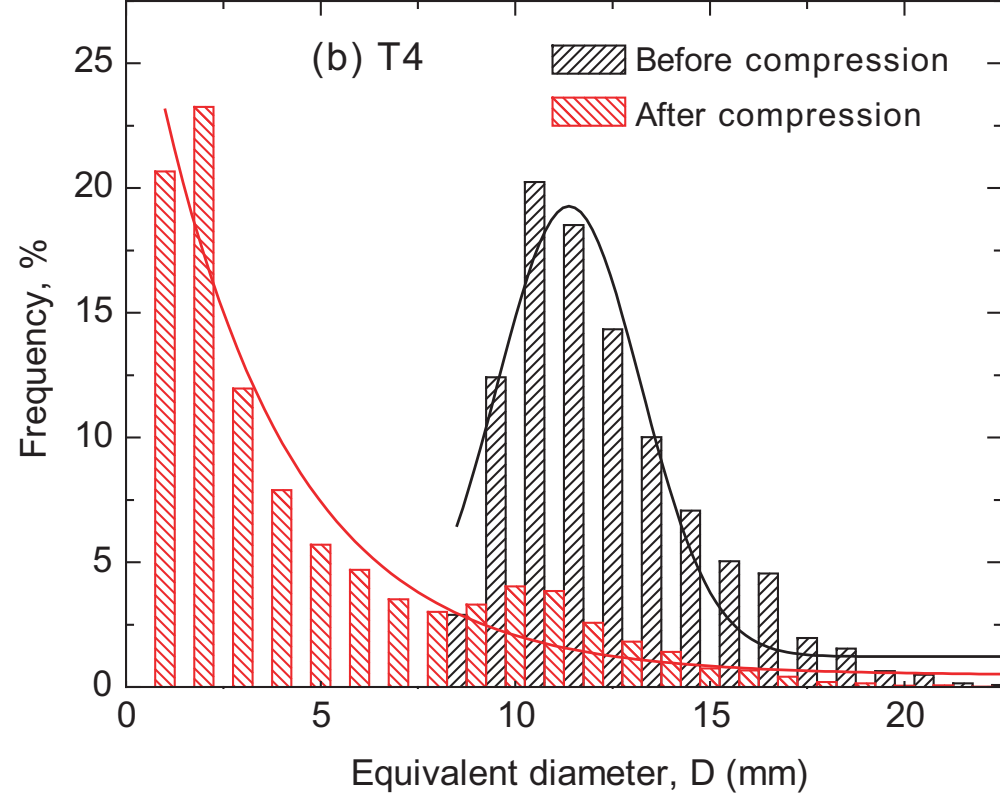
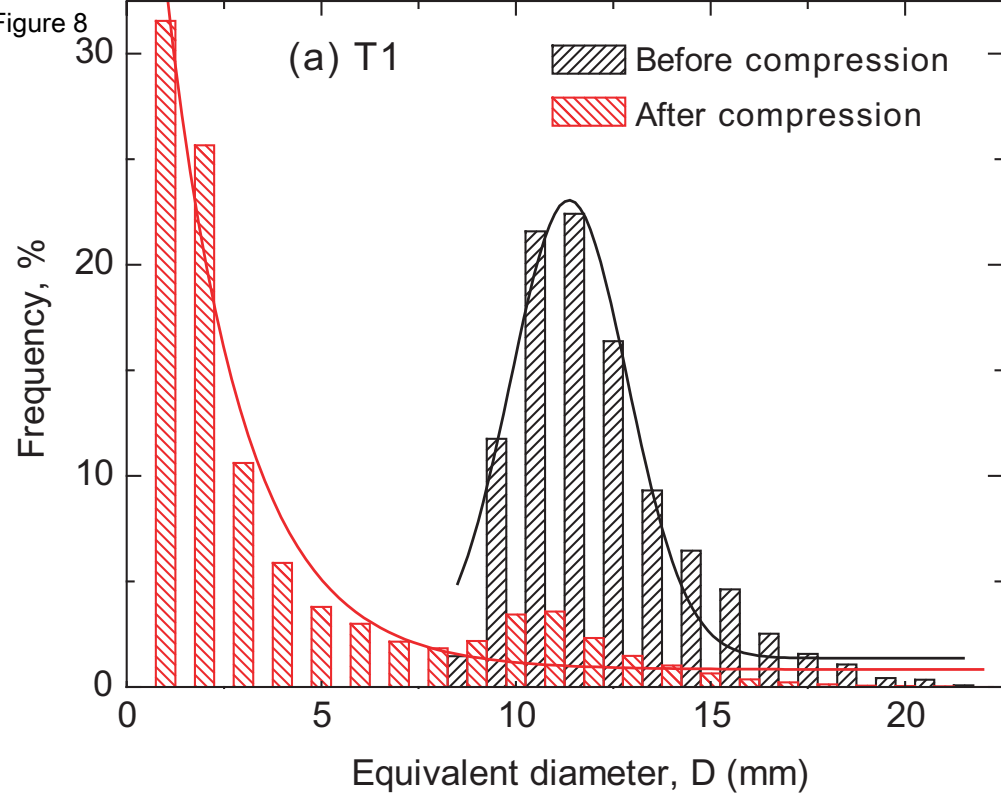
(c)

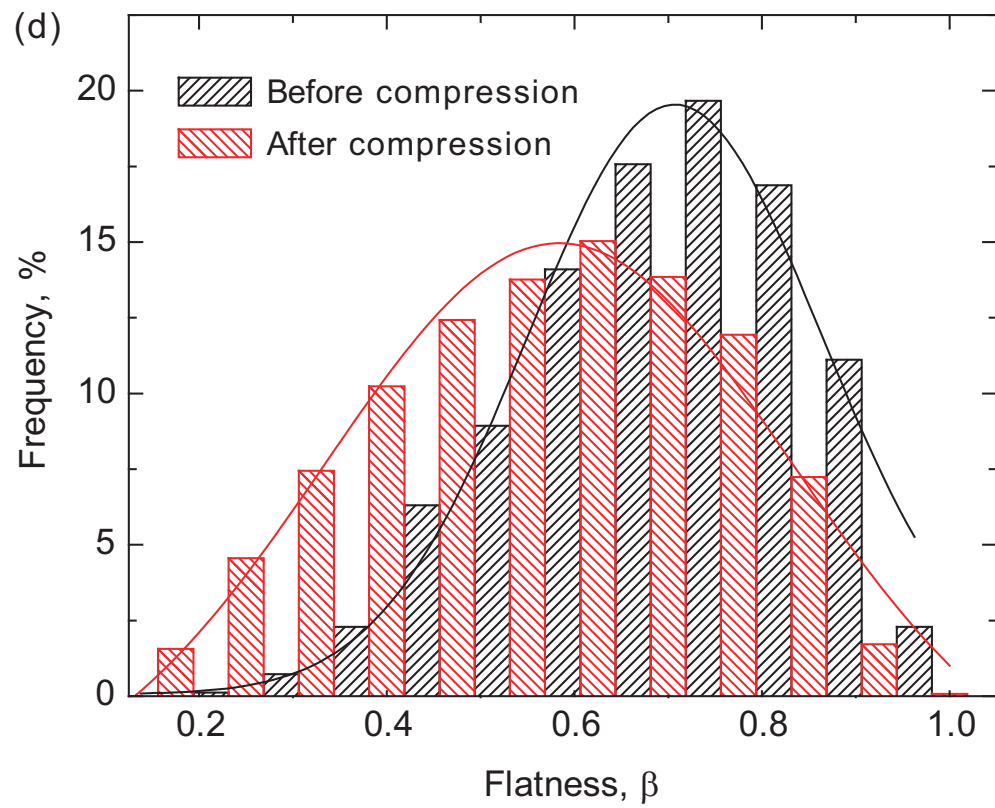
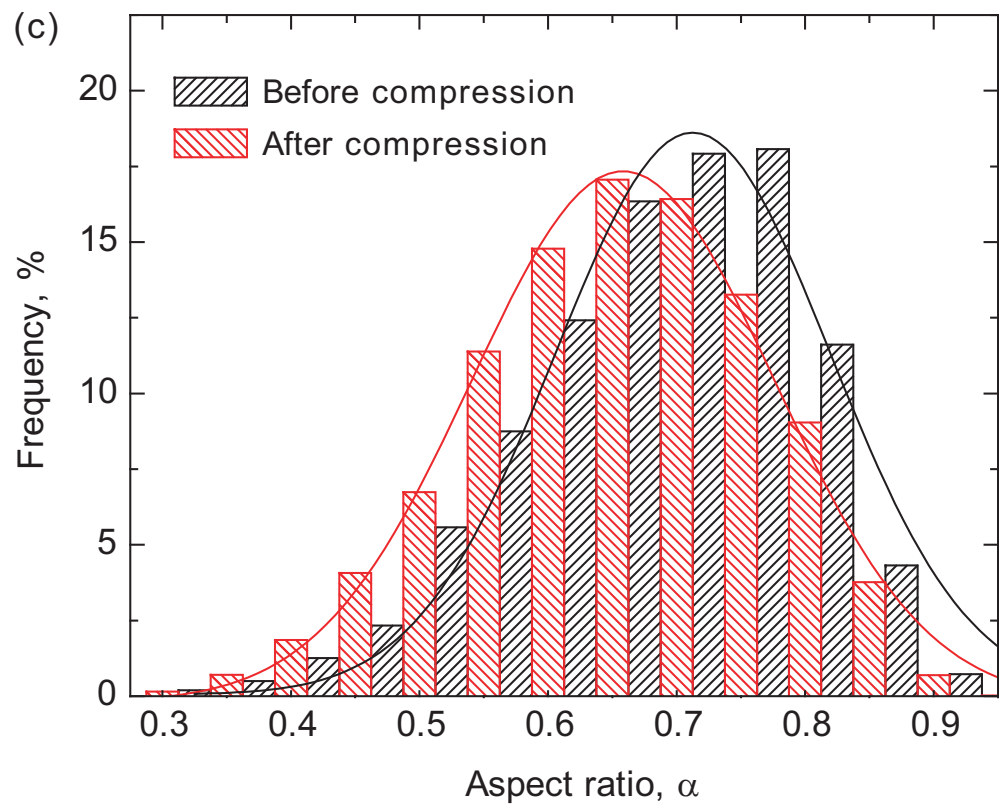
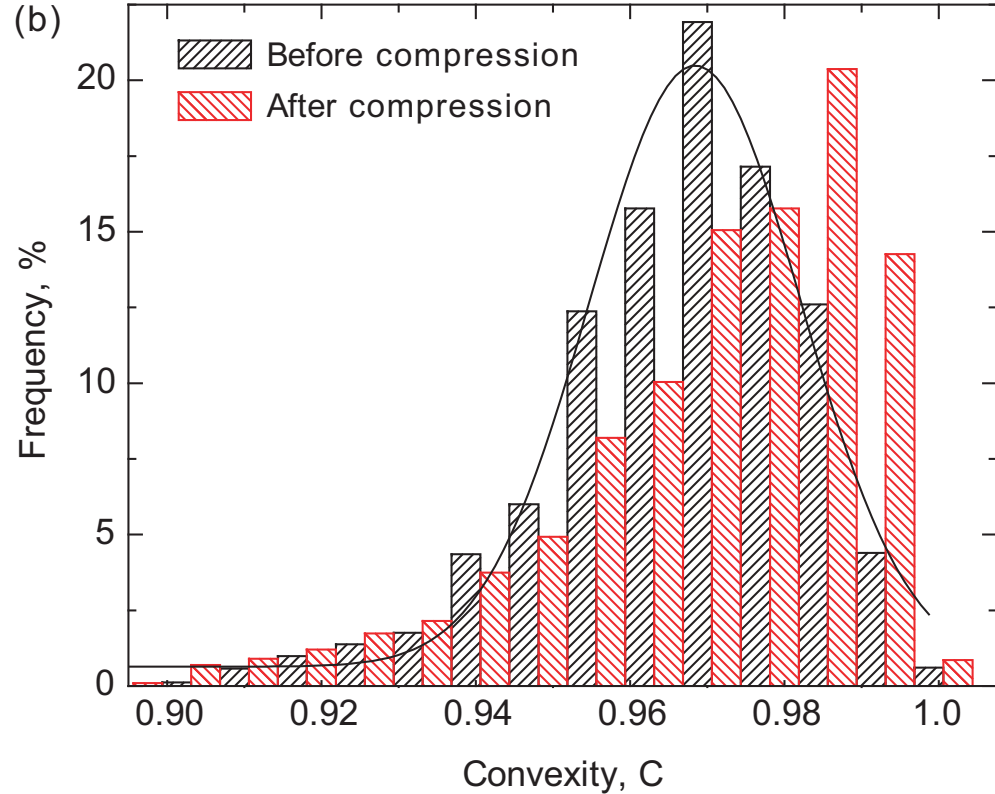
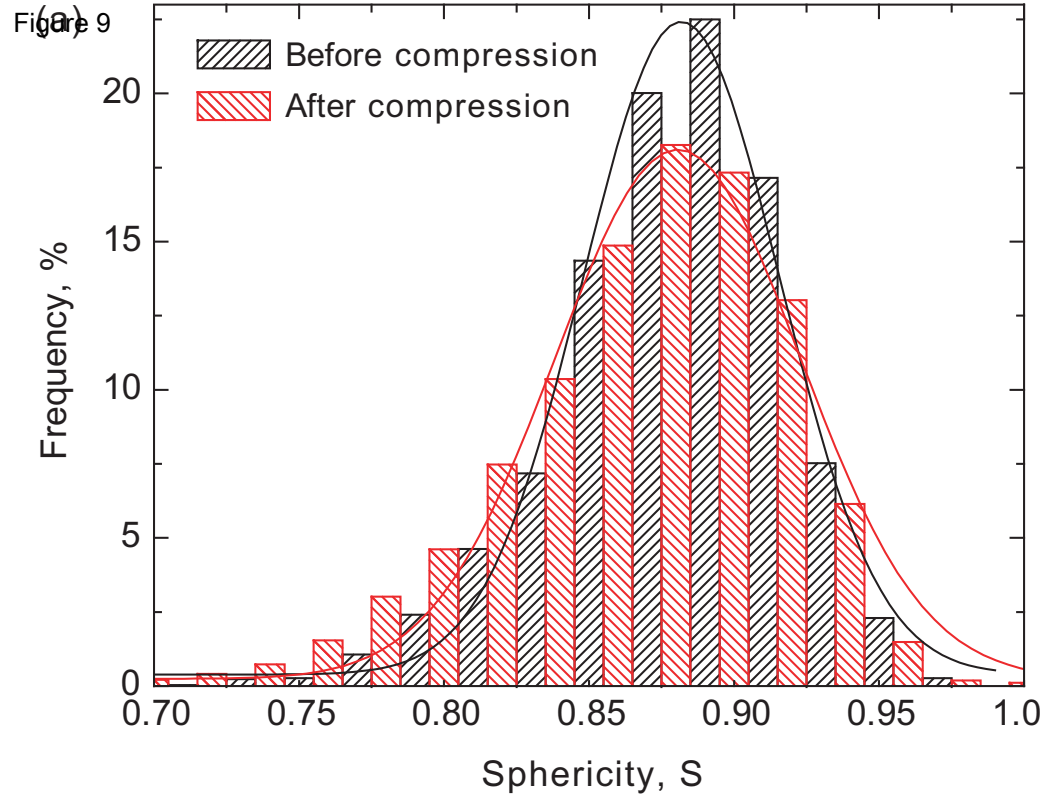


(d)



Figure 8





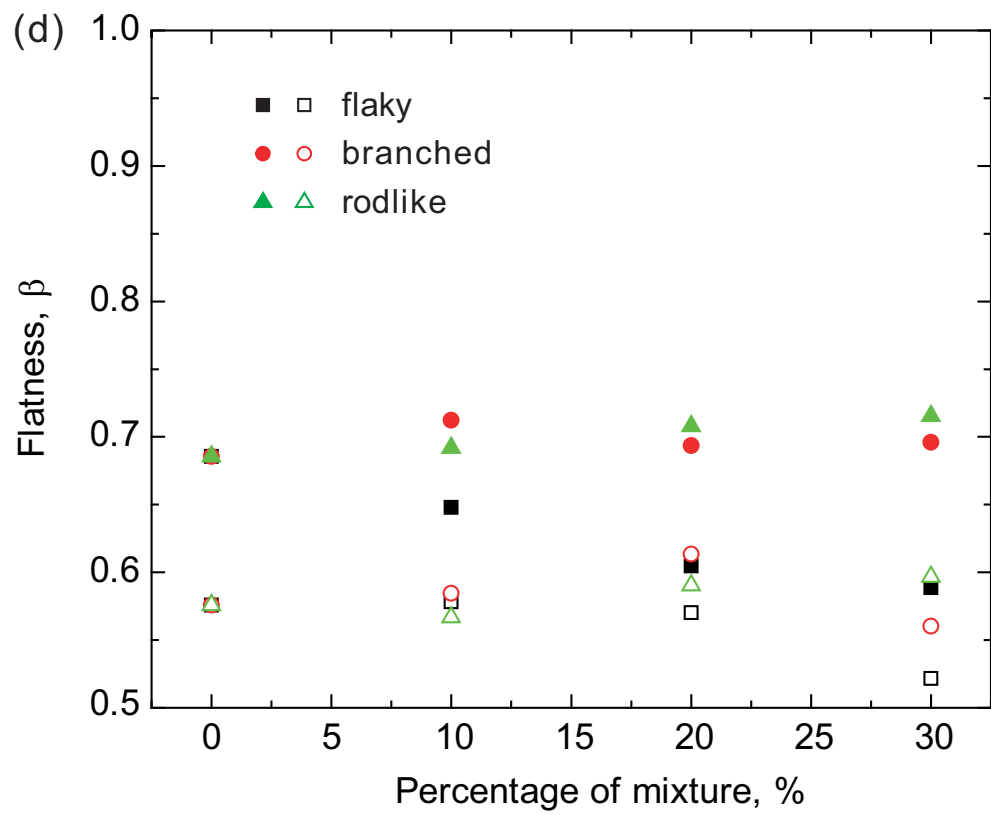
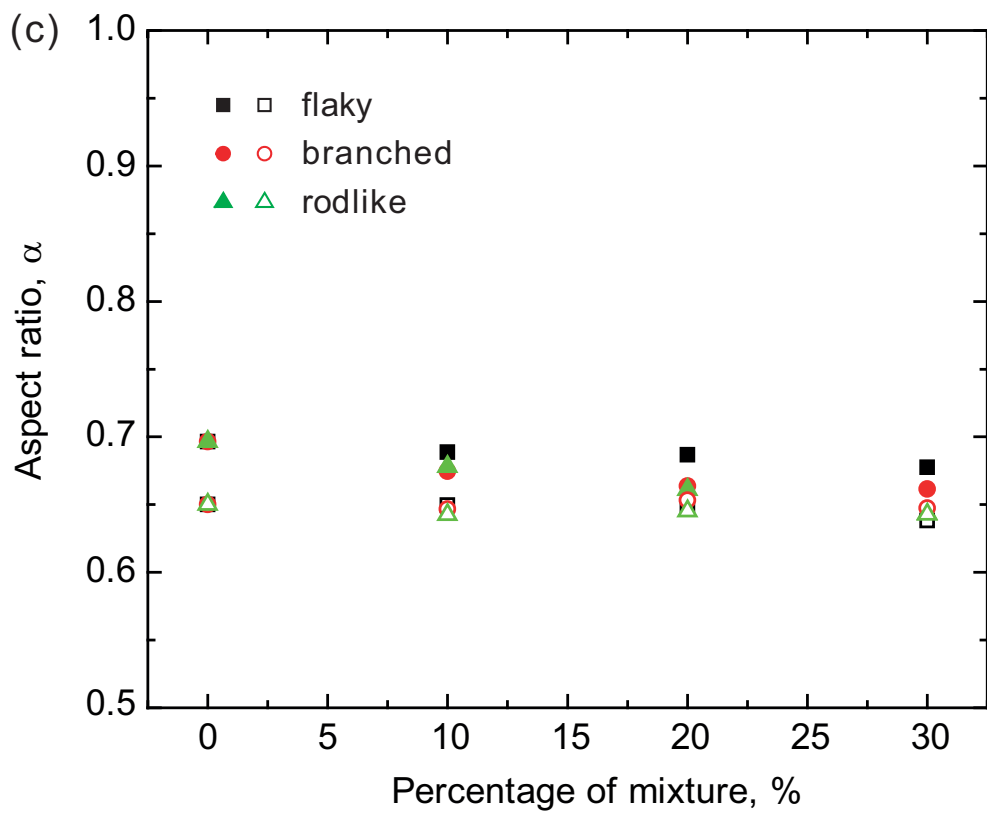
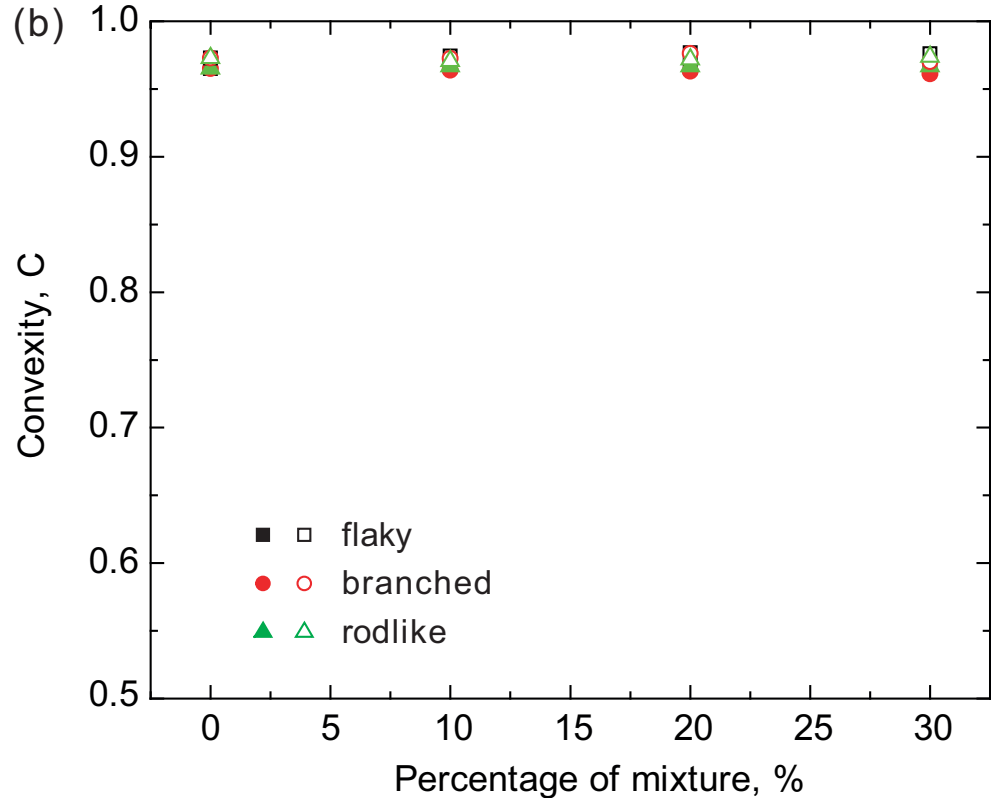
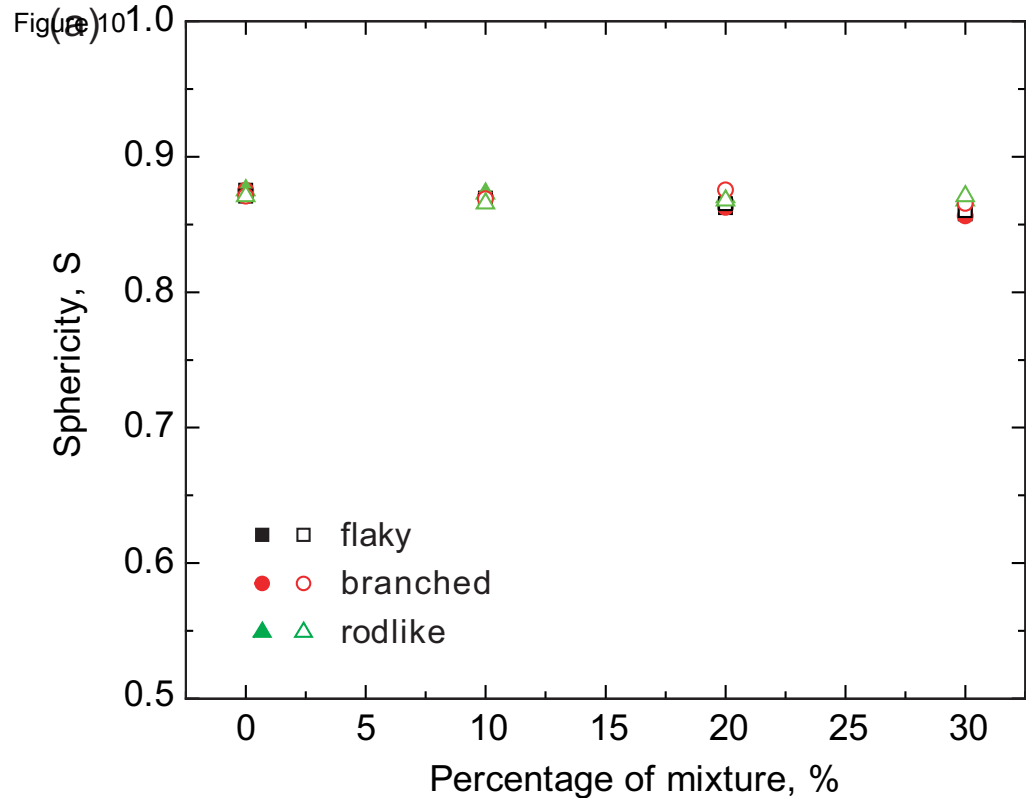


Figure 11

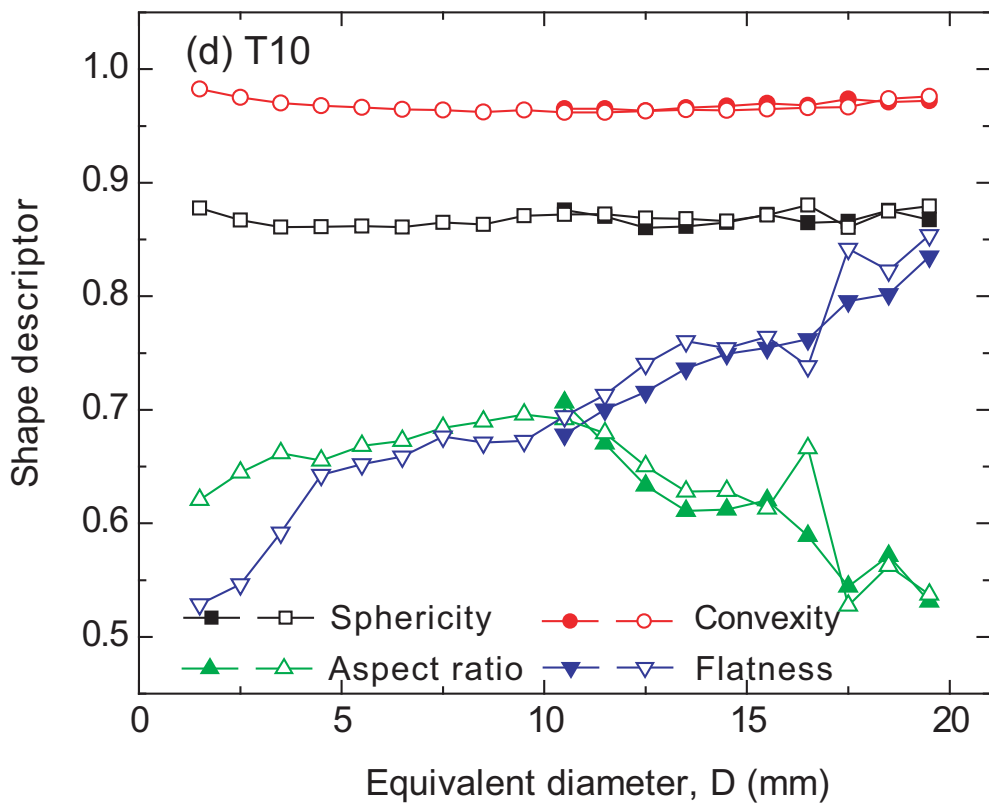
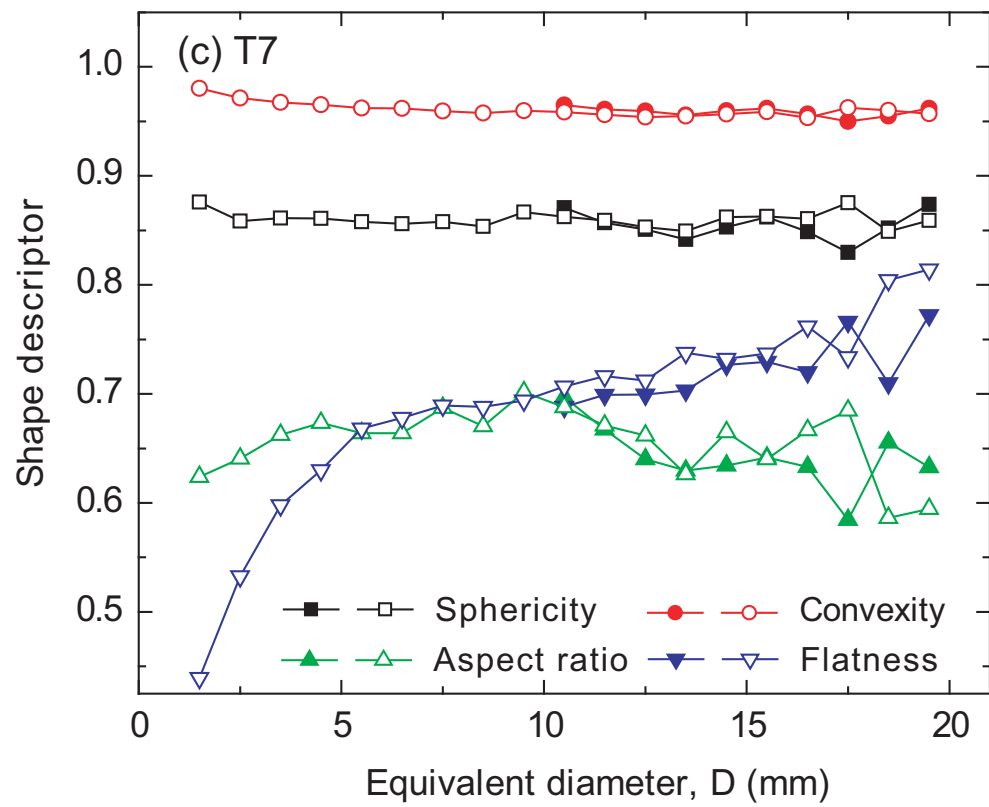
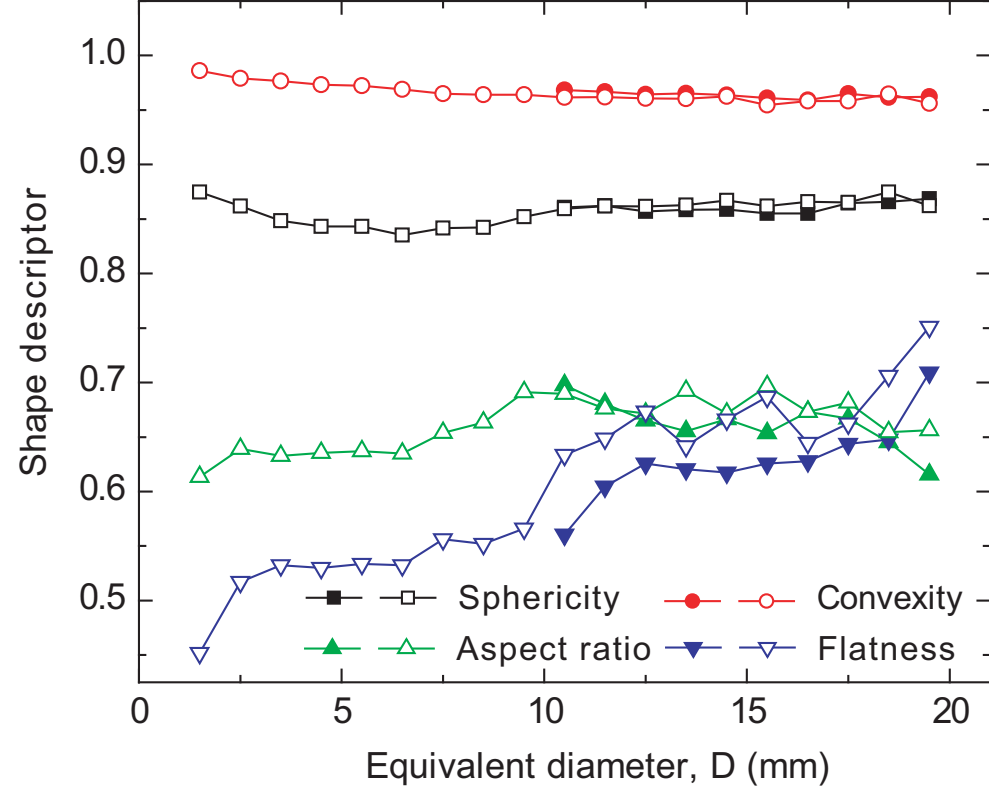
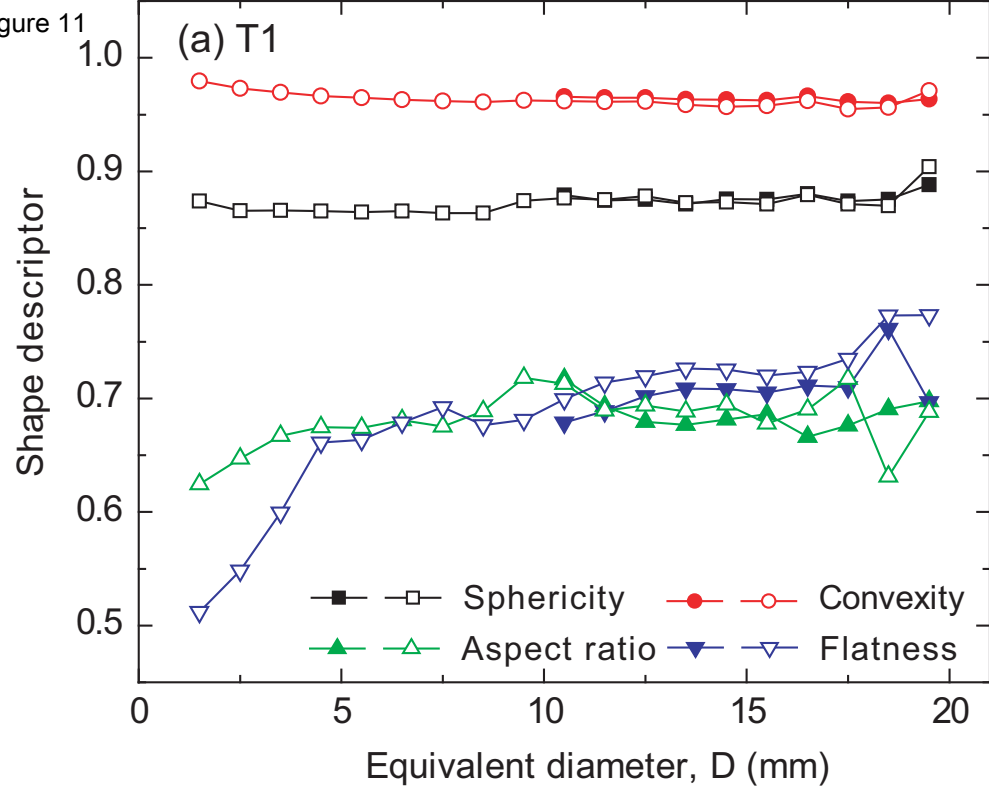


Figure 12

